

Special  
Collection

# Oxidative Photopolymerization of 3,4-Ethylenedioxythiophene (EDOT) via Graphitic Carbon Nitride: A Modular Toolbox for Attaining PEDOT\*\*

Cansu Esen,<sup>[a]</sup> Markus Antonietti,<sup>[a]</sup> and Baris Kumru<sup>\*[a]</sup>

Conductive polymers find key applications ranging from optoelectronics and OLEDs to conductive composite materials. The synthesis of conductive polymers from monomers, such as thiophene derivatives, pyrroles and aniline, mainly relies on oxidative polymerization, and the processing of so-formed (insoluble) polymers is a major issue that needs to be

addressed. In the present work, oxidative photopolymerization of 3,4-ethylenedioxythiophene (EDOT) by visible light employing the metal-free semiconductor graphitic carbon nitride (g-CN) is presented. Two main reaction pathways based on g-CN content are described, and the formation of processable oligo-EDOT is demonstrated.

## 1. Introduction

Conductive polymers have introduced a novel dimension in polymer science, that is the capability to manufacture organic matter that conducts electrons.<sup>[1]</sup> Ever since, many conductive polymers have been presented, such as polyacetylene,<sup>[2]</sup> polyaniline,<sup>[3]</sup> polypyrrole,<sup>[4]</sup> and thiophene based polymers.<sup>[5]</sup> The application range of such conductive materials span from OLED materials, thermoelectrics, photovoltaics, electrochemistry, optoelectronics and biomedical.<sup>[6]</sup> 3,4-ethylenedioxythiophene (EDOT) has withdrawn special attention as even in the doped state it exhibits high conductivity as well as stability.<sup>[7]</sup> Polymerization of EDOT can be performed via three methods: coupling reaction of halogen substituted EDOT derivatives,<sup>[8]</sup> electrochemical polymerization,<sup>[9]</sup> and oxidative polymerization by oxidative agents.<sup>[10]</sup> The so-formed PEDOT is a black insoluble material with very restricted processability.<sup>[11]</sup> For example, electrochemical polymerization grants formation of PEDOT only on conductive surfaces.<sup>[12]</sup> To overcome this problem, researchers have added poly(styrene sulfonic acid) (PSS) during oxidative polymerization of EDOT catalyzed via FeCl<sub>3</sub> or Fe(Tos)<sub>3</sub> in water, which provides a water dispersible PSS doped PEDOT material.<sup>[13]</sup> Despite the processability is gained via PSS addition, the polymer properties are lowered compared to pure PEDOT analogue.<sup>[14]</sup> Other methodologies

that would endorse the synthesis of a processable PEDOT are certainly welcomed.

Graphitic carbon nitride (g-CN, g-C<sub>3</sub>N<sub>4</sub>) is a semiconductor polymer that is mainly composed of nitrogen and carbon atoms in a conjugated framework, such as tri-s-triazine.<sup>[15]</sup> g-CN represents a family of materials with facile tunability such as bandgap, work function, surface properties and elemental doping in the framework.<sup>[16,17]</sup> Furthermore, its non-toxic and highly stable character together with the synthesis from low cost and abundant precursors (i.e. melamine, urea, dicyandiamide) place g-CN as a new generation semiconductor to be investigated in fields such as photocatalytic water splitting, CO<sub>2</sub> reduction, pollutant degradation and light-induced sanitization.<sup>[18–23]</sup> For instance, Kui Li et al. recently reported a graphitic carbon nitride integrated multicomponent nanocomposite via dual ligand adopted hierarchical-MOFs which shows enhanced H<sub>2</sub> generation in water.<sup>[24]</sup> Furthermore, the integration of g-CN into polymer systems is expanding.<sup>[25]</sup> Embedding a charge transfer mediator consisting of conductive polymer as a heterostructure onto g-CN resulted in a highly efficient dual noble-metal-free cocatalyst designed by Kui Li and co-workers.<sup>[26]</sup> So far g-CN has been employed as a heterogeneous photoinitiator for polymer synthesis,<sup>[27,28]</sup> alternatively g-CN dispersions were utilized for hydrogel synthesis<sup>[29]</sup> and for heterophase polymerizations.<sup>[30]</sup> Also the combination of g-CN with conductive polymers is full of opportunities,<sup>[31]</sup> however this method is restricted by the means of processing techniques. Formation of g-CN-PEDOT:PSS composites reported in the literature are obtained through blending method to enhance the photocatalytic efficiencies,<sup>[32,33]</sup> however, g-CN assisted PEDOT synthesis was not yet described. In this manuscript, the utilization of g-CN as a photoredox type photoinitiator for oxidative photopolymerization of EDOT via visible light will be presented. Two different pathways to promote oligo-EDOT processing at different g-CN concentration will be demonstrated, i.e. processable oligomeric liquid oligo-EDOT (Path A) and in situ g-CN doped oligo-EDOT composites (Path B) (Scheme 1).

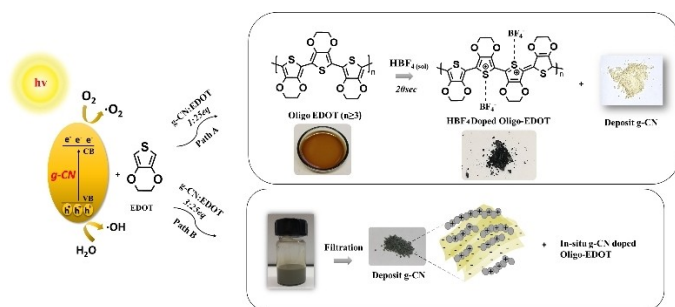
[a] C. Esen, Prof. Dr. M. Antonietti, Dr. B. Kumru  
Department of Colloid Chemistry  
Max Planck Institute of Colloids and Interfaces  
Am Mühlenberg 1, 14424 Potsdam (Germany)  
E-mail: baris.kumru@mpikg.mpg.de

[\*\*] PEDOT = Poly(3,4-ethylenedioxythiophene).

Supporting information for this article is available on the WWW under <https://doi.org/10.1002/cptc.202100046>

An invited contribution to the "GDCh and ChemPhotoChem: 5-Year Anniversary" Special Collection

© 2021 The Authors. ChemPhotoChem published by Wiley-VCH GmbH. This is an open access article under the terms of the Creative Commons Attribution License, which permits use, distribution and reproduction in any medium, provided the original work is properly cited.



Scheme 1. Oxidative photopolymerization of EDOT via g-CN.

## 2. Results and Discussion

g-CN photocatalyst was synthesized by thermal condensation of cyanuric acid-melamine supramolecular complex as reported in the literature<sup>[34]</sup> to obtain a yellow powder material. Following that, g-CN in different proportions (100 or 300 mg) are mixed with 2 mL EDOT and stirred under visible light irradiation for 24 h at room temperature. A simple filtration is sufficient to separate the catalyst from the product, thus both can be independently analyzed. Catalyst amount granted two synthetic pathways, path A (100 mg g-CN) promotes dark-brown oligo-EDOT formation together with unaltered g-CN powder, and path B (300 mg g-CN) exhibits in situ g-CN oligo-EDOT formation, with oligo-EDOT finally deposited on g-CN powder by electric charge compensation.

The crystal structures of all g-CN powders (pristine catalyst is denoted as g-CN, g-CN isolated from path A is denoted as g-CN R1 and g-CN isolated from path B is denoted as g-CN R2) can be investigated via powder XRD. All three samples demonstrate the two typical peaks corresponding to (100) and (002) planes at 13° and 27°, representing intralayer spacing and interlayer sheet-sheet spacing, respectively (Figure S1a).<sup>[34]</sup> However, a significant enhancement on the (002) plane intensity was observed for g-CN R2 which can be ascribed to a oligo-EDOT deposition. g-CN possesses a strong light absorbance between 270–450 nm (Figure S1b) thus rendering it suitable for a visible light-driven photoredox reactions.<sup>[35]</sup> As depicted in Figure S1b, the spectrum of pristine g-CN overlays with the one of g-CN R1 thus indicating that the g-CN R1 remained photophysically unchanged after photopolymerization initiation. In the case of g-CN R2, an intensified and broader absorbance was recorded which confirms strong electronic coupling by conjugation of oligo-EDOT on the g-CN surface. In addition to that, oligo-EDOT deposition on g-CN R2 can also be observed from thermogravimetric analysis which shows enhanced thermal stability in comparison with other g-CN samples (Figure S1c). FT-IR analysis was carried out for all g-CN samples, and similar spectra for all three samples were obtained, C–N conjugated ring vibrations in the range of 1255–1630 cm<sup>-1</sup>, triazine motif vibration around 810 cm<sup>-1</sup> and –NH<sub>2</sub> + –OH bands around 3250 cm<sup>-1</sup> (Figure S1d). Furthermore, elemental compositions of all g-CN samples were determined via combustive elemental analysis, which confirms the similarity between pristine g-CN and g-CN R1, but an enhanced sulfur

content of g-CN R2 arises from oligo-EDOT deposition which also allows the quantification of its content (Table S1). Following that, homogeneously distributed sulfur and oxygen content linked to a oligo-EDOT deposition on g-CN R2 was also observed by elemental mapping analysis via EDX (Figure S2). At last, Tauc plots derived from UV absorption of CM, and CM R1 and CM R2 at specified range are presented in Figure S3 with calculated bandgap values at g-CN absorption maximum. As expected, CM (2.89 eV) and CM R1 (2.84 eV) exhibited quite similar band gap values unlike CM R2 (2.76 eV) which was based on shifted absorption spectrum caused by oligo-EDOT deposition.

After the oxidative photopolymerization of colorless EDOT, the resulting liquid oligo-EDOT (after separation of g-CN) undergoes significant darkening compared to EDOT. Generally, pitch black color of oligo-EDOT arises from its fully oxidized state, however a photoredox synthesis cannot donate a full oxidation, so a linear oligo-EDOT with a moderate oxidation is obtained in the present case. In order to get more insight about eventual molecular weight, UV-vis spectra were applied as inspired by the literature (Figure S4a).<sup>[36–38]</sup> The significant bathochromic shift on UV-vis spectrum from 450 nm to 650 nm is explicated as a sign of an increased molecular weight of EDOT based on extended conjugated units. It should be noted that, a reductive pre-treatment is subjected to conduct neutral stated PEDOT in literature however, as the procedure is compatible for simultaneously assisted PEDOT coupled materials for example PEDOT:PSS or PEDOT-Lignosulfonate but not to our conditions, it was not performed before the measurement and by this reason, an intensified peak at 389.31 nm detected as a sign for oligo-EDOT formation instead of a significant red-shifting. Moreover, when the reaction went under argon atmosphere, the intensity of the peak, which was attained to oligo-EDOT formation, has lowered as a correspond to the lack of oxygen. Following that, photoluminescence spectra of oligo-EDOT shown broad emission with  $\lambda_{\text{max}}$  417 nm as a sign of  $\pi$ - $\pi^*$  transition in its as-formed conjugated system (Figure S4b).

Not only by the means of color, but an enhanced viscosity of oligo-EDOT compared to EDOT was measured (Figure S5), which hints towards oligomer formation. Furthermore, structural investigations of liquid oligo-EDOT were performed via FT-IR analysis (Figure 1). The C=C and C–C stretching modes of

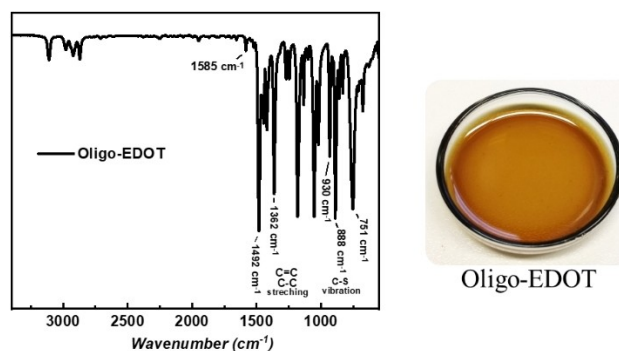


Figure 1. FT-IR spectrum of oxidatively photopolymerized oligo-EDOT along with its digital image (after catalyst separation).

the thiophene ring are found at 1362, 1443, and 1492  $\text{cm}^{-1}$ , the peak at 1585  $\text{cm}^{-1}$  indicates the conjugation in polymeric structure, the ether ethylenedioxy stretching modes are displayed at 1180 and 1047  $\text{cm}^{-1}$  and finally the C–S vibration modes appear at 751, 888 and 930  $\text{cm}^{-1}$ .<sup>[39]</sup> All signals and the assignments are in good agreement with literature, underlining the formation of oligo-EDOT.

It is known that monomers such as EDOT, aniline and pyrrole are prone to oxidative polymerization and even further an in situ polymerization based upon redox relay mechanism assisted with non-noble metal can result in a highly efficient catalyst for solar conversion as reported by Kui Li and colleagues.<sup>[40]</sup> In our case, we have attempted to obtain a possible reaction mechanism. Similar reaction in the absence of an air does not yield a polymer product, and the same reaction under oxygen feeding is much more effective, which hints that the oxygen is the species to be reduced to close the photo-redox cycle (Figure S6). Likewise, reaction in the absence of a photocatalyst does not yield any oligomerized product confirmed via unaltered EDOT absorption. The main factor to consider in EDOT photopolymerization is the matching bandgaps, a milestone article which employed perovskite quantum dots for the PEDOT synthesis was only possible when trimerEDOT was employed as a monomer, and the main mechanism was based on photoformed holes.<sup>[41]</sup> Mixture without light irradiation shows no change under the same conditions, which indicates the necessity for the strong oxidation power of the light activated hole in the valence band of carbon nitride to drive the polymerization. From the photo-redox chemistry point of view, another question is the fate of the photoformed excited electrons. As EDOT polymerization forms cationic species,<sup>[42]</sup> charge balancing is important for propagation. A similar scenario is observed when PSS is added to EDOT polymerization, on one side it provides an enhanced aqueous processability, and on the other side it renders a charge balance thus facilitating the polymerization.<sup>[43]</sup> It is expected that in our case, photoformed holes take a hydrogen from EDOT molecule providing a radical cation. Excited electron activates dissolved oxygen to form  $\text{O}_2^{\bullet-}$ , which balances the positive charge (through  $^-\text{OOH}$ ) and EDOT molecules undergo radical-radical coupling therefore forming an oligomerization, as depicted in proposed reaction mechanism (Figure S6). Advantage of photoredox compared oxidative polymerization is that in the present case, one obtains a PEDOT that is not fully oxidized as no real negative counterions are present. Fabrication of such PEDOT must possess a significant affinity to dissolved negative charges. In order to investigate that, we have performed doping of oligo-EDOT (2 mL) via aqueous  $\text{HBF}_4$  solution (0.1 mL). As expected, only in 20 seconds, significant darkening takes place, and a viscous as well as dispersed material is formed.

Regarding FT-IR analysis of post-doped oligo-EDOT, the broadened peak from 3612 to 3153  $\text{cm}^{-1}$  along with the reduced signal at 3106  $\text{cm}^{-1}$  can be attributed to the integration of the counterion due to doping into the polymeric structure. The bathochromic shift with a broadening from 1550 to 1410  $\text{cm}^{-1}$  can be considered as a result of de-doping by

reversing the charge carriers through the presence of dopant ion (Figure 2a, Figure S7).<sup>[44]</sup> The structural information of doped oligo-EDOT was investigated via powder XRD that exhibits low-intensity diffraction peaks indicating the amorphous nature of the polymeric material at  $12.8^\circ$  with respect to two-dimensional arrangement of oligo-EDOT and dopant ion, whereas the sharp peak at  $24.1^\circ$  represents the ring stacking of the stiff aromatic polymer chains (Figure 2b).<sup>[45]</sup>

The broad UV-vis absorption band of doped oligo-EDOT is typical for organic electron conductors. Furthermore, an intensified peak from 478 nm with  $\lambda_{\text{max}}$  662 nm to 530 nm can be correlated to  $\pi$ - $\pi^*$  transition of the thiophene ring, and the shoulder from 547 nm to 759 nm can be attributed to the oxidized state of oligo-EDOT according to literature (Figure 2c).<sup>[46]</sup>

In order to quantify the thermal stability of post-doped oligo-EDOT, thermogravimetric analysis is performed. The first weight loss occurring from  $58^\circ\text{C}$  to  $180^\circ\text{C}$  can be attributed to the evaporation of residual water molecules (from  $\text{HBF}_4$  solution) in the sample, following that the step-wise weight losses eventuated in about 40 wt% residual mass at  $800^\circ\text{C}$  (Figure 2d).

It is known that the thermal decomposition of oligo-EDOT takes place between  $300^\circ\text{C}$  and  $400^\circ\text{C}$  as reported in publications,<sup>[47]</sup> and employing doped oligo-EDOT as a carbon precursor seems to be very appealing. Therefore, a carbonization of doped oligo-EDOT was conducted at  $800^\circ\text{C}$  in a nitrogen protected oven. After the carbonization process, doped oligo-EDOT and the resulting carbonaceous material were analyzed via combustive elemental analysis. As expected, carbon content has increased significantly after carbonization, as well as a decrease in hydrogen content was found. The most significant element in this case is sulfur, and a surprisingly high sulfur content (16.5 wt.%) of for an  $800^\circ\text{C}$  treated carbon

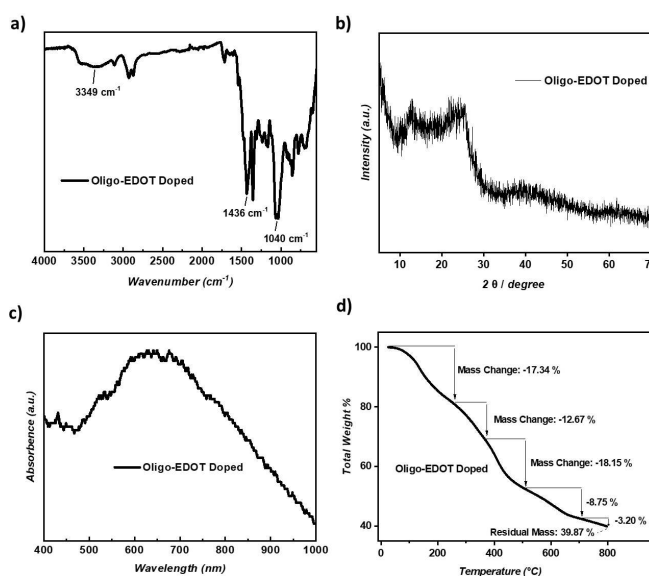


Figure 2. a) FT-IR spectrum, b) XRD profile, c) UV-Vis spectrum, d) thermogravimetric analysis of post-doped oligo-EDOT.

product was observed, that can be of significant interest in catalysis (Table 1).<sup>[48]</sup>

During carbonization, doped oligo-EDOT precursor effortlessly granted an access for a homogeneous film deposition on the walls of the crucible and on the lid (Figure S8), which can be a practically useful observation to decipher the potential of doped oligo-EDOT as a carbon film precursor. SEM characterization and EDX mapping of the carbon powder exhibits homogeneous distribution of the atoms without any compartmentalization (Figure S9).

One of the major drawbacks of PEDOT is its processability, especially when applied-scale coating and film formation are required.<sup>[49]</sup> Fabrication of a liquid PEDOT and post-doping brings a significant solution for these issues, and for that we have performed a coating on a glass, metal coin and ITO coated glass slide surfaces via dip-coating. SEM images of post-doped oligo-EDOT (a powder obtained from a coating, Figure 3 a1) and its coating on a glass (Figure 3 a2) exhibited a perfect planar morphology, and successful coating could be confirmed. Besides its simple processability, the coated film also possesses an adequate resistance against water over 5 days, and no peeling was observed (Figure S10). Since the surface coating process performed effectively, sheet/surface resistivity measurement can be the next step accordingly. Post-doped oligo-EDOT and in situ g-CN doped oligo-EDOT were applied on ITO coated glass slide via dip coating, and their resistivities were verified via a two-probe multimeter and compared with pristine ITO coated surface (Figure S11). The results showed that the sheet resistivity of post-doped oligo-EDOT film (20.1  $\Omega/\text{sq}$ ) is lower than ITO surface resistivity (36.8  $\Omega/\text{sq}$ ) which in reverse means that the conductivity is enhanced with the applied oligo-EDOT

**Table 1.** Combustive elemental analysis results of doped oligo-EDOT and its carbonized product.

Sample	C [%]	N [%]	S [%]	H [%]
Doped oligo-EDOT	47.68	0.54	20.65	3.78
Carbonized oligo-EDOT	71.34	1.1	16.56	0.8

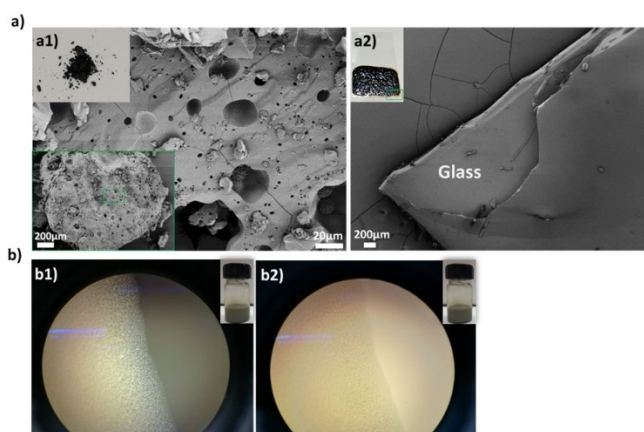


**Figure 3.** a) Scanning electron microscopy images of powder post-doped oligo-EDOT (a1) and coated post-doped oligo-EDOT coating on glass (a2). b) Optical microscopy images of in situ g-CN doped oligo-EDOT under polarized (b1) and normal light (b2).

film on ITO coated glass surface. This also confirms that resulting oligo-EDOT and its further post-doping level are eligible to accelerate surface conductivity, explicitly. On the other hand, in situ g-CN doped oligo-EDOT exhibited higher surface resistivity (1.706  $\Omega/\text{sq}$ ) measured on higher sensitivity scale that indicates a restricted electron movement over the sample compared to post-doped PEDOT (Figure S11c).

As a final statement for all these promising results that have been stated so far, combining the described procedures with elaborated coating technologies could be of high interest for industrial-scale conductive polymer applications.

Increasing g-CN content for oxidative photopolymerization of EDOT again reveals an unusual composite system. As discussed above, the product from this reaction (g-CN R2) is a g-CN coated with oligo-EDOT, thus presenting a straightforward mechanism to form g-CN oligo-EDOT composite materials. As oligo-EDOT remains on g-CN surface despite long purification processes, we assume direct charge conjugation between a negatively charged g-CN and the positively charged doped oligo-EDOT. This can be related to the ability of g-CN to store and buffer a rather high amount of photogenerated electrons and the coupled negative charges,<sup>[50]</sup> which then instead of a low molecular weight counterion- compensate the positive charge of oligo-EDOT in the hybrid structure. Such hybrids are very stable, as they cannot be resolved by a simple oxidation or reduction process, as then always the opposite charge is left unbalanced, and only the addition of special ion pairs can destabilize the structure. In addition to stability, presence of oxygen might affect the storage stability of as-prepared oligo-EDOT therefore, it is recommended to store freshly synthesized samples with an inert gas purge.

g-CN is well-dispersed in the polymer media and dopes oligo-EDOT in addition. In-situ g-CN doped oligo-EDOT is captured by optical microscopy under normal and polarized light (Figure 3 b1, b2) which confirms the dispersion of g-CN particles in oligo-EDOT phase. The fact that spontaneous charge transfer at the semiconductor-semiconductor occurs according to their work function is a classic phenomenon of semiconductor physics, but rather rarely used for electronically diverse aromatic semiconductors in solution or dispersion.<sup>[51]</sup> One can say that the electronically very diverse oligo-EDOT and g-CN undergo a mutual doping effect, potentially highly accelerated by light irradiation.

### 3. Conclusion

The metal-free semiconductor g-CN can be used for the oxidative photopolymerization of EDOT with visible light. A one-pot synthetic procedure in the presence of oxygen was presented, and the high selectivity of g-CN oxidation allows for the neutral oligo-EDOT formation but stops before oxidative doping when other ions are absent. Throughout this process no polymer precipitation is obtained, films can be formed, which then can be post-doped to generate conductive and insoluble films and coatings. On the other hand, utilization of excess g-CN facilitates the formation of a hybrid heterojunction

material where oligo-EDOT is deposited on g-CN powder through surface polaron formation. Furthermore, organic oligo-EDOT phase is in situ doped with g-CN nanosheets through a negative surface charge, thus offering a novel avenue of semiconductor heterojunctions. Overall, a simple light-induced procedure to manufacture highly functional materials enabled by g-CN will be of high impact in polymer chemistry and catalysis fields.

## Experimental Section

### Materials

3,4-Ethylenedioxythiophene (EDOT, 97%, Sigma-Aldrich), cyanuric acid (98%, Sigma-Aldrich), dimethyl sulfoxide (DMSO, 99.9% ACS reagent, Sigma), melamine (99%, Fluka), indium tin oxide (ITO) coated glass slide (Rectangular, 8–12  $\Omega$ /sq, Sigma-Aldrich), tetrafluoroboric acid (HBF<sub>4</sub>, 48% in water, Sigma-Aldrich). 50 W LED chips (Foxpic High Power 50 W LED Chip Bulb Light DIY White 3800LM 6500 K) were connected to a self-made circuit and cooling system.

### Synthesis of g-CN

5.0 g of cyanuric acid and 5.0 g of melamine were mixed with 100 mL distilled water and shaken overnight to form cyanuric acid-melamine supramolecular precursor.<sup>[34]</sup> After centrifugation at 6000 rpm for 15 minutes, a precipitate was collected. A precipitate was dried overnight at 60 °C under vacuum. The dried product was transferred into a capped crucible and put into N<sub>2</sub> protected oven at 550 °C for 4 h, with a heating rate of 2.3 °C/min. The resulting yellow powder is denoted as g-CN and it is well grinded prior to use.

### Photopolymerization of EDOT

100 mg g-CN and 2 mL EDOT are mixed in a vial and sonicated in a sonic bath for 10 minutes. Following that, the vial is placed in front of a 50 W visible light source with a continuous stirring for 24 h at room temperature (29 °C was measured after 24 h of irradiation). oligo-EDOT can be obtained by filtering the photocatalyst (Yield: 75 %). Filtered photocatalyst is extensively washed with DMSO and ethanol and dried in an oven. Reused catalyst is denoted as g-CN R1.

### Control reaction-photopolymerization of EDOT in the absence of air

100 mg g-CN and 2 mL EDOT are mixed in a vial, nitrogen or argon flux was applied for 30 minutes, the mixture is then sonicated in a sonic bath for 10 minutes. Following that, the vial is placed in front of a 50 W visible light source with a continuous stirring for 24 h at room temperature.

### Control reaction-photopolymerization of EDOT in the absence of light

100 mg g-CN and 2 mL EDOT are mixed in a vial, the mixture is then sonicated in a sonic bath for 10 minutes. Following that, continuous stirring for 24 h at room temperature in the dark was applied.

### Doping oligo-EDOT

0.1 mL HBF<sub>4</sub> solution is poured over 2 mL liquid oligo-EDOT in a petri dish, and significant darkening as well as spontaneous dispersion formation are observed in 20 seconds upon mixing. Resulting dark material is dried in an oven at 60 °C for 4 h to obtain doped oligo-EDOT solid material.

### Photopolymerization of EDOT via excess g-CN

300 mg g-CN and 2 mL EDOT are mixed in a vial and sonicated in a sonic bath for 10 minutes. Following that, the vial is placed in front of a 50 W visible light source with a continuous stirring for 24 h at room temperature (30 °C was measured after 24 h of irradiation). Resulting composite was characterized further by the means of both solid and liquid phase. Filtered photocatalyst is extensively washed with DMSO and ethanol and dried in an oven. Reused catalyst is denoted as g-CN R2.

### Doped oligo-EDOT coating processes

Indium tin oxide (ITO) coated glass slide was treated to a wet chemical etching/cleaning process; firstly washed with aqueous HCl then immersed in isopropanol and sintered at 250 °C for 2 h. After the cleaning process, post-doped-oligo-EDOT and in situ g-CN doped oligo-EDOT were manually coated on ITO surfaces and placed in an oven at 70 °C overnight. A coin and a glass surface were immersed in a liquid doped oligo-EDOT, and coated surfaces are placed in an oven at 60 °C for 2 h.

### Carbonization of Post-doped oligo-EDOT

460 mg HBF<sub>4</sub> doped oligo-EDOT was placed in a capped crucible and put into N<sub>2</sub> protected chamber furnace at 800 °C for 30 minutes with a heating rate of 5 °C/min. The resulting material is a solid black powder.

### Characterization

Fourier transform infrared (FT-IR) spectra were acquired on a Nicolet iS 5 FT-IR spectrometer. Solid-state ultraviolet-visible (UV-vis) spectroscopy was performed via a Cary 500 Scan spectrophotometer equipped with an integrating sphere. Photoluminescence spectra of ethanol, pure oligo-EDOT and oligo-EDOT/EtOH (55 mg/2 mL) placed in 10 mm path length quartz cuvette were recorded by a Horiba FluoroMax-4, integration time 0.2–1 s, and slits apertures 10 nm. All the fluorescence spectra were recorded using excitation at 295 nm. Obtained spectra values reported as either S1c in units of cps or by S/R mode with units of cps/microAmp in which are corrected S1c and R1c detectors. X-ray diffraction (XRD) patterns of all g-CN samples and powder HBF<sub>4</sub> doped oligo-EDOT were obtained by using a Bruker D8 Advance X-ray diffractometer via Cu K $\alpha$  radiation. Scanning electron microscopy (SEM) was performed using a JSM-7500F (JEOL) microscope equipped with an Oxford Instruments X-Max 80 mm<sup>2</sup> detector for the determination of post-doped oligo-EDOT and its coating onto glass. Viscosity measurements were performed at room temperature with a changing shear rate between 1–20 s<sup>-1</sup>. Thermogravimetric analysis (TGA) was performed via TG 209 Libra from Netzsch in nitrogen atmosphere with heating rate 10 Kmin<sup>-1</sup> using aluminum crucible for post-doped oligo-EDOT. Conductivity measurement of post-doped oligo-EDOT coated on indium tin oxide coated glass slide was performed via PEAQTECH 3335 DMM two-probe multimeter 600 V, 100 Hz, 20Mohm with an illuminated LCD display. Optical microscopy images were taken by Olympus BX41.

## Acknowledgements

The authors thank the Max Planck Society for funding and providing the infrastructure. Antje Volkel is greatly acknowledged for TGA and elemental analysis measurements. We thank Dr. Paolo Giusto for the fluorescence measurement. Ursula Lubahn is acknowledged for the immense help in the lab. Open access is granted by Project DEAL. Open access funding enabled and organized by Projekt DEAL.

## Conflict of Interest

The authors declare no conflict of interest.

**Keywords:** colloids · conducting materials · photocatalysis · polymerization · semiconductors

- [1] Y. Shi, L. Peng, Y. Ding, Y. Zhao, G. Yu, *Chem. Soc. Rev.* **2015**, *44*, 6684–6696.
- [2] P. Bujak, I. Kulszewicz-Bajer, M. Zagorska, V. Maurel, I. Wielgus, A. Pron, *Chem. Soc. Rev.* **2013**, *42*, 8895–8999.
- [3] B. Kumru, N. Bıçak, *Macromol. Symp.* **2015**, *352*, 42–45.
- [4] A. L. Pang, A. Arsad, M. Ahmadipour, *Polym. Adv. Technol.* **2020**.
- [5] M. E. Cinar, T. Ozturk, *Chem. Rev.* **2015**, *115*, 3036–3140.
- [6] T. Nezakati, A. Seifalian, A. Tan, A. M. Seifalian, *Chem. Rev.* **2018**, *118*, 6766–6843.
- [7] L. Groenendaal, F. Jonas, D. Freitag, H. Pielartzik, J. R. Reynolds, *Adv. Mater.* **2000**, *12*, 481–494.
- [8] L. G. Mercier, M. Leclerc, *Acc. Chem. Res.* **2013**, *46*, 1597–1605.
- [9] T. Lindfors, Z. A. Boeva, R.-M. Latonen, *RSC Adv.* **2014**, *4*, 25279–25286.
- [10] C. Jiang, G. Chen, X. Wang, *Synth. Met.* **2012**, *162*, 1968–1971.
- [11] M. N. Gueye, A. Carella, J. Faure-Vincent, R. Demadrille, J.-P. Simonato, *Prog. Mater. Sci.* **2020**, *108*, 100616.
- [12] V. Castagnola, C. Bayon, E. Descamps, C. Bergaud, *Synth. Met.* **2014**, *189*, 7–16.
- [13] X. Fan, W. Nie, H. Tsai, N. Wang, H. Huang, Y. Cheng, R. Wen, L. Ma, F. Yan, Y. Xia, *Adv. Sci.* **2019**, *6*, 1900813.
- [14] J. Ouyang, *Displays.* **2013**, *34*, 423–436.
- [15] G. Zhang, Z.-A. Lan, X. Wang, *Chem. Sci.* **2017**, *8*, 5261–5274.
- [16] B. Kumru, M. Antonietti, *Adv. Colloid Interface Sci.* **2020**, *283*, 102229.
- [17] M. Majdoub, Z. Anfar, A. Amedlous, *ACS Nano.* **2020**, *14*, 12390–12469.
- [18] P. Xia, B. Zhu, J. Yu, S. Cao, M. Jaroniec, *J. Mater. Chem. A* **2017**, *5*, 3230–3238.
- [19] S. Cao, J. Yu, *J. Phys. Chem. Lett.* **2014**, *5*, 2101–2107.
- [20] P. Giusto, B. Kumru, J. Zhang, R. Rothe, M. Antonietti, *Chem. Mater.* **2020**, *32*, 7284–7291.
- [21] G. Liao, F. He, Q. Li, L. Zhong, R. Zhao, H. Che, H. Gao, B. Fang, *Prog. Mater. Sci.* **2020**, *112*, 100666.
- [22] Z. Zhou, Y. Zhang, Y. Shen, S. Liu, Y. Zhang, *Chem. Soc. Rev.* **2018**, *47*, 2298–2321.
- [23] J. Ji, J. Wen, Y. Shen, Y. Lv, Y. Chen, S. Liu, H. Ma, Y. Zhang, *J. Am. Chem. Soc.* **2017**, *139*, 11698–11701.
- [24] M.-L. Xu, L.-W. Liu, K. Wang, Y.-C. Dou, K. Li, X. Cheng, F.-M. Zhang, *J. Mater. Chem. A* **2020**, *8*, 22124–22133.
- [25] Q. Cao, B. Kumru, M. Antonietti, B. V. K. J. Schmidt, *Macromolecules.* **2019**, *52*, 4989–4996.
- [26] K. Li, Y.-Z. Lin, K. Wang, Y. Wang, Y. Zhang, Y. Zhang, F.-T. Liu, *Appl. Catal. B* **2020**, *268*, 118402.
- [27] Q. Fu, Q. Ruan, T. G. McKenzie, A. Reyhani, J. Tang, G. G. Qiao, *Macromolecules.* **2017**, *50*, 7509–7516.
- [28] S. Dadashi-Silab, M. A. Tasdelen, B. Kiskan, X. Wang, M. Antonietti, Y. Yagci, *Macromol. Chem. Phys.* **2014**, *215*, 675–681.
- [29] B. Kumru, V. Molinari, M. Hilgart, F. Rummel, M. Schaeffler, B. V. K. J. Schmidt, *Polym. Chem.* **2019**, *10*, 3647–3656.
- [30] N. Yandrapalli, T. Robinson, M. Antonietti, B. Kumru, *Small* **2020**, *16*, 2001180.
- [31] Y. Xu, W. Lei, J. Su, J. Hu, X. Yu, T. Zhou, Y. Yang, D. Mandler, Q. Hao, *Electrochim. Acta* **2018**, *259*, 994–1003.
- [32] Z. Xing, Z. Chen, X. Zong, L. Wang, *Chem. Commun.* **2014**, *50*, 6762–6764.
- [33] W. Wu, A. Ali, R. Jamal, M. Abdulla, T. Bakri, T. Abdiryim, *RSC Adv.* **2019**, *9*, 34691–34698.
- [34] M. Shalom, S. Inal, C. Fettkenhauer, D. Neher, M. Antonietti, *J. Am. Chem. Soc.* **2013**, *135*, 7118–7121.
- [35] G. Dong, Y. Zhang, Q. Pan, J. Qiu, *J. Photochem. Photobiol. C* **2014**, *20*, 33–50.
- [36] C. D. Spicer, M. A. Booth, D. Mawad, A. Armgarth, C. B. Nielsen, M. M. Stevens, *Chem.* **2017**, *2*, 125–138.
- [37] Q. Fu, Y. Li, X. Wang, Q. Li, F. Wang, R. Yang, *J. Mater. Chem. C* **2020**, *8*, 17185–17193.
- [38] Y. Li, H. Lou, F. Wang, Y. Pang, X. Qiu, *ChemistrySelect* **2019**, *4*, 11406–11412.
- [39] S. V. Selvaganes, J. Mathiyarasu, K. L. N. Phani, V. Yegnaraman, *Nano-scale Res. Lett.* **2007**, *2*, 546.
- [40] T. Li, J.-D. Cui, L.-M. Gao, Y.-Z. Lin, R. Li, H. Xie, Y. Zhang, K. Li, *ACS Sustainable Chem. Eng.* **2020**, *8*, 13352–13361.
- [41] K. Chen, X. Deng, G. Dodekatos, H. Tüysüz, *J. Am. Chem. Soc.* **2017**, *139*, 12267–12273.
- [42] D. Mantione, I. D. agua, A. Sanchez-Sanchez, D. Mecerreyes, *Polymer* **2017**, *9*, 354.
- [43] M. Mueller, M. Fabretto, D. Evans, P. Hojati-Talemi, C. Gruber, P. Murphy, *Polymer.* **2012**, *53*, 2146–2151.
- [44] Y. Wang, K. Cai, X. Yao, *ACS Appl. Mater. Interfaces.* **2011**, *3*, 1163–1166.
- [45] Q. Zhao, R. Jamal, L. Zhang, M. Wang, T. Abdiryim, *Nanoscale Res. Lett.* **2014**, *9*, 557.
- [46] Y. Osman, R. Jamal, A. Rahman, F. Xu, A. Ali, T. Abdiryim, *Synth. Met.* **2013**, *179*, 54–59.
- [47] S. Bontapalle, S. Varughese, *Polym. Degrad. Stab.* **2020**, *171*, 109025.
- [48] J. P. Paraknowitsch, A. Thomas, J. Schmidt, *Chem. Commun.* **2011**, *47*, 8283–8285.
- [49] Y. Wen, J. Xu, *J. Polym. Sci. Part A* **2017**, *55*, 1121–1150.
- [50] A. Savateev, Y. Markushyna, C. M. Schuesslbauer, T. Ullrich, D. M. Guldi, M. Antonietti, *Angew. Chem. Int. Ed.* **2021**, *60*, 7436–7443.
- [51] K. Xu, H. Sun, T.-P. Ruoko, G. Wang, R. Kroon, N. B. Kolhe, Y. Puttisong, X. Liu, D. Fazzi, K. Shibata, C.-Y. Yang, N. Sun, G. Persson, A. B. Yankovich, E. Olsson, H. Yoshida, W. M. Chen, M. Fahlman, M. Kemerink, S. A. Jenekhe, C. Müller, M. Berggren, S. Fabiano, *Nat. Mater.* **2020**, *19*, 738–744.

Manuscript received: February 27, 2021  
 Revised manuscript received: April 29, 2021  
 Accepted manuscript online: May 3, 2021  
 Version of record online: May 26, 2021